Astronomical Refraction

Michael E. Thomas and Richard I. Joseph

Astronomical observations near the horizon have historically been made for naval navigation and for determining the time of sunset. Recent applications include near-horizon daytime scene simulation to support infrared search and track and infrared seeker studies. The ray path of the setting or rising Sun can be highly distorted near the horizon, and it is seldom rectilinear. An accurate model of atmospheric refraction must include the observer's altitude as well as range, frequency, and atmospheric pressure and temperature. At infrared through ultraviolet frequencies, refractivity depends strongly on the vertical temperature profile, and an explicit relationship between refractivity and temperature can be obtained. This article describes a refraction model we developed that closely reproduces the profile of the setting Sun.

INTRODUCTION

The real part of the atmospheric index of refraction is a function of pressure, temperature, and frequency. Many interesting low-altitude refractive effects exist because of tropospheric variations in density and water-vapor partial pressure as a function of position. Atmospheric refraction is divided into three categories: astronomical, terrestrial, and geodesic. Astronomical refraction addresses ray-bending effects for objects outside the Earth's atmosphere relative to an observer within the atmosphere. Terrestrial refraction considers the case when both object and observer are within the Earth's atmosphere. Geodesic refraction is a special case of terrestrial refraction where the object and observer are at low altitudes, as is commonly the case in surveying.

Two components of a complete atmospheric refraction model are (1) a representation of the index of refraction of the atmosphere as a function of pressure, temperature, and frequency, and (2) a description of the ray path. This article presents an improved general numerical procedure for computing astronomical observations as a function of the inclination angle in the visible/infrared portion of the electromagnetic spectrum. The model is applied to observations of sunset.

REFRACTIVITY OF A STANDARD ATMOSPHERE

Because of the abundance of nitrogen and oxygen, the contributions of those elements dominate the refractivity of a dry atmosphere. Nitrogen and oxygen molecules have no infrared bands of importance to the refractive index, so that only electronic bands need to be considered for a model valid from millimeter waves to the ultraviolet. On the basis of the work of Edlen,[1] a simple semi-empirical model for the dry air refractivity, N_{dry}, is given by

$$\begin{aligned} N_{dry} &= (n_{dry} - 1) \times 10^6 \\ &= (776.2 + 4.36 \times 10^{-8} \nu^2) P_{dry} / T , \end{aligned} \quad (1)$$

where n_{dry} is the dry air index of refraction, ν is the wavenumber (reciprocal of the wavelength) in cm^{-1}, P_{dry} is the total dry air pressure in kilopascals, and T is the temperature in kelvins. This model is valid at altitudes where the mixing ratio between oxygen and nitrogen is fixed (<100 km) and from 0.2 to 2,000 μm (5 to 50,000 cm^{-1}); it also compares well with other models.[2,3]

By using the hydrostatic equation for total pressure, and given the temperature profile, the altitude dependence z' can also be included in the dry air refractivity as follows:

$$N_{dry}(\nu, T(z')) = (776.2 + 4.36 \times 10^{-8}\nu^2) \times \frac{P_{dry}(z'_0)}{T(z')} \exp\left[-\frac{mg}{k_B}\int_{z'_0}^{z'} \frac{dz''}{T(z'')}\right], \quad (2)$$

where z'_0 is the observer altitude above sea level, m is the average molecular mass of a dry atmosphere, g is gravitational acceleration, and k_B is Boltzmann's constant. For altitudes up to 100 km, mg/k_B is 34.16 K/km. The vertical temperature profile for the 1976 U.S. Standard Atmosphere has a lapse rate in the troposphere of −6.5 K/km (first 11 km) and a constant temperature in the stratosphere (11 to 20 km). Above 20 km, the index of refraction is close to 1, and details of the temperature dependence become less important. For this reason, the constant temperature of the stratosphere is applied to all higher altitudes. The representation of refractivity as a function of altitude in Eq. 2 is a simple yet useful relationship for ray path modeling.

RAY PATH MODEL

Because the index of refraction depends on density, and the density of the atmosphere strongly depends on altitude, light propagating in the atmosphere is bent (typically toward lower altitudes or regions of higher density). The density of the atmosphere does not vary greatly in the horizontal direction and, hence, only the vertical structure needs to be considered. For an observer at altitude z'_0 viewing an astronomical object at an altitude z' above a spherically stratified Earth as illustrated in Fig. 1, the refracted path $\theta(z', \delta)$ for $\delta \geq 0$ is given by[4]

$$\theta(z', \delta) = \int_{z'_0}^{z'} \frac{dz''}{(R_E + z'')\sqrt{\frac{[n(z'')(R_E + z'')]^2}{[n(z'_0)(R_E + z'_0)]^2}\sec^2\delta - 1}}, \quad (3)$$

where $n(z'')$ is the index of refraction as a function of altitude, R_E is the Earth's radius, and δ is the inclination (or elevation) angle. Equation 3 has been applied by astronomers and navigators for many years to correct for atmospheric refraction. An approximate solution has been obtained by Garfinkel[5] for a standard atmosphere.

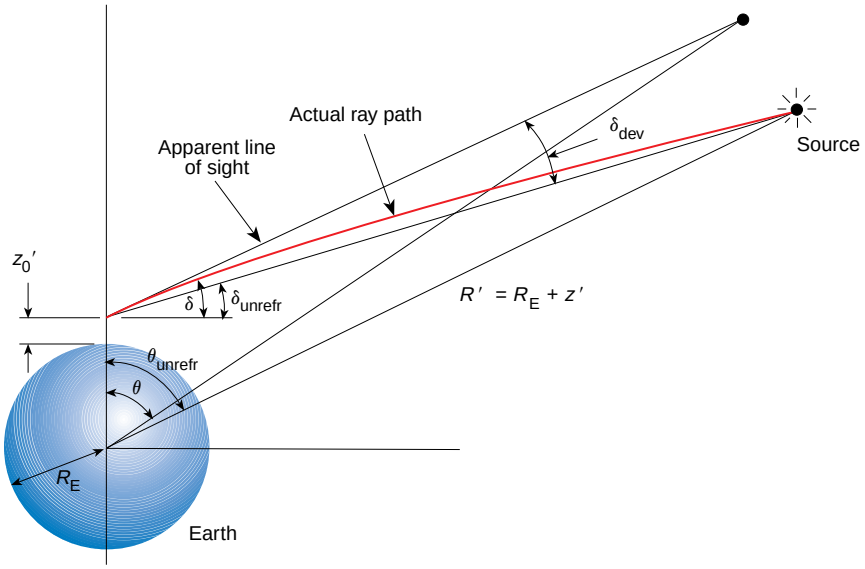

Figure 1. Illustration of the angle of deviation for viewing an astronomical object by an observer at altitude z'_0 and inclination angle δ within a spherically stratified atmosphere surrounding the Earth. θ, refracted ray path; θ_{unrefr}, unrefracted ray path.

For general index of refraction vertical profiles, however, numerical integration techniques are necessary to obtain the refracted path. Simpson's rule is commonly applied (one important user of this approach is the U.S. Naval Observatory).[6] The vertical temperature profile is often constructed with a piecewise continuous representation, which produces cusps at boundaries between layers. Unfortunately, numerical instability problems occur at these cusps in the vertical temperature profile. This representation also limits the general applicability of the method since the integrand must be segmented between the locations of the cusps. A reasonably efficient and stable numerical approach is to apply Gauss-Chebyshev quadrature numerical integration to the preceding integral. A simple variable substitution leads to the following equivalent form for Eq. 3:

$$\theta(Z(z',\delta),\delta) = \int_{Z(z',\delta)}^{\cos\delta} \frac{1}{\sqrt{1-Z'(z'',\delta)^2}} \times \frac{dZ'}{\dfrac{dn(Z'(z'',\delta))}{dz''}\dfrac{C(\delta)}{Z'(z'',\delta)}+1}, \tag{4}$$

where the following substitutions have been made:

$$C(\delta) = \frac{n(z_0')(R_E + z_0')}{\sec\delta},$$

$$Z(z',\delta) = \frac{n(z_0')(R_E + z_0')}{n(z')(R_E + z')}\cos\delta,$$

$$Z'(z'',\delta) = \frac{n(z_0')(R_E + z_0')}{n(z'')(R_E + z'')}\cos\delta.$$

This form of the integrand also points out an integrable singularity in the leading factor for the important case when $\delta = 0$. Although not a problem for an exact calculation, it can be a problem for a numerical calculation. Because the leading factor is the weighting function for Chebyshev polynomials, the chosen numerical approach avoids the singularity. Furthermore, the preceding integral can be solved exactly when the index of refraction is constant, which is essentially the case above the Earth's atmosphere ($n = 1$). Within the atmosphere, a numerical approach is needed. The implementation of a 200 term Gauss-Chebyshev quadrature from z_0' to z_1' (= 100 km), and the exact solution for constant index from 100 km to z', lead to the following approximate form:

$$\theta(z',\delta) = \sum_{i=1}^{200}\frac{\pi f(Z_i'(z_1',\delta),\delta)}{200} + \sin^{-1}\left[\frac{R_E + z_0'}{R_E + z_1'}n(z_0')\cos\delta\right] - \sin^{-1}\left(\frac{R_E + z_1'}{R_E + z'}\cos\delta\right), \tag{5}$$

where the first argument of the function f is defined as

$$Z_i'(z_1',\delta) = \frac{\cos\delta + Z(z_1',\delta)}{2} + \frac{\cos\delta - Z(z_1',\delta)}{2}\cos\left[\frac{(2i-1)}{400}\pi\right],$$

and f is given by

$$f(Z_i',\delta) = \frac{\sqrt{[Z_i' - Z(z_1',\delta)](\cos\delta - Z_i')}}{\sqrt{1-Z_i'^2}} \times \frac{1}{\left[\dfrac{dn(z''(Z'))}{dz''}\right]_{Z_i'}\dfrac{C(\delta)}{Z_i'}+1}.$$

Of particular interest is the computation of the deviation angle δ_{dev} as a function of the inclination angle δ, as defined in Fig. 1. The unrefracted ray path θ_{unrefr} can be determined exactly from Eq. 3 for n constant. The result is

$$\theta_{unrefr}(z',\delta) = \sin^{-1}[\cos(\delta)] - \sin^{-1}\left[\frac{R_E + z_0'}{R_E + z'}\cos(\delta)\right]. \tag{6}$$

The difference between the unrefracted and refracted inclination angles determines the deviation angle, $\delta_{dev}(\delta)$. It is given in terms of unrefracted and refracted θ angles by

$$\delta_{dev}(z_0',\delta) = \theta_{unrefr}(z',\delta) - \theta(z',\delta) + \frac{R_E + z_0'}{R_E + z'}[\sin(\theta_{unrefr}) - \sin(\theta)]. \tag{7}$$

RESULTS

We checked the results given by Eq. 7 by computing the angular deviation of an astronomical object observed through a standard atmosphere as a function of elevation angle. The temperature profile is that of the 1976 U.S. Standard Atmosphere as described earlier and is used in conjunction with Eq. 2 to provide a model of the vertical refractivity. Using this profile, we found that Eq. 7 closely reproduces the results listed in Table 1 for an observer near sea level.[7]

It is interesting to note that the angular extent of the Sun is 32 arcmin, and the maximum deviation or refraction correction angle for a standard atmosphere is 34.5 arcmin; thus, even though the setting Sun is below the geometrical horizon, it can be observed. Note also from Table 1 that the refraction correction angle varies across the angular extent of the Sun near the horizon. Thus, the Sun appears more flattened at the bottom than at the top. This point is illustrated in Fig. 2, which shows a photograph of the setting Sun and the corresponding computed shape based on Eq. 7 at a wavenumber of 20,000 cm^{-1} (0.5 μm). The photograph was taken during the summer at an altitude of about 130 m. The temperature at the observer was about 31°C with a lapse rate of −8 K/km.

Another example with the Sun at a higher elevation angle and the observer at a lower altitude is shown in Fig. 3, which compares the observed rim of the setting Sun in a photograph from Greenler's book[8] with the computed shape of the Sun. A standard atmosphere is used in this case with an observer at 10 m. The different shapes in the two figures are closely represented by the astronomical refraction model.

Table 1. Refraction deviation angles for an observer at sea level, for inclination angles of astronomical lines of sight through a standard atmosphere.[7]

Observed inclination, δ (deg min)	Refraction deviation (min)	Observed inclination, δ (deg)	Refraction deviation (min)
0 00	34.5	11	4.9
15	31.4	12	4.5
30	28.7	13	4.1
45	26.4	14	3.8
1 00	24.3	15	3.6
15	22.5	16	3.3
30	20.9	17	3.1
45	19.5	18	2.9
2 00	18.3	19	2.8
15	17.2	20	2.6
30	16.1	25	2.1
45	15.2	30	1.7
3 00	14.4	35	1.4
4 30	10.7	50	0.8
5	9.9	55	0.7
6	8.5	60	0.6
7	7.4	65	0.5
8	6.6	70	0.4
9	5.9	80	0.2
10	5.3	90	0.0

CONCLUSIONS

Typical variations in the atmospheric index of refraction cause an uncertainty in refraction correction angles as listed in Table 1, with a root-mean-square deviation of 0.16 arcsec.[9] Also, the standard atmosphere refractivity profile seldom occurs in the lower troposphere, and significant differences from the standard deviation angle do occur. (Commonly observed mirage effects testify to the variability of atmospheric conditions.[8,10,11] Measurements of such distorted images can be used for remote sensing of the atmosphere.[12]) Therefore, a flexible model capable of handling nonstandard refractivity profiles and different observer altitudes is needed.

Futhermore, dispersion of the refractive index causes the refraction correction angle to vary slightly for different frequencies (colors). Thus, the setting Sun disappears one color at a time: red first, blue last. This refractive condition explains the observance of the "green spot"[9] at sunset when the horizon is exceptionally clear in a standard atmosphere. (Note: The popular but rarely observed "green flash" is a result of ducting phenomena.[10,13]) Dispersion effects can be computed from Eqs. 2 and 7 by including the frequency dependence of the index of refraction. For example, Greenler's book contains a photograph of Venus near the horizon.[8] The color separation of the image is distinct and estimated to be 0.006° from red to green. This value is consistent with the computed angular separation, based on Eq. 7, obtained using the 1976 U.S. Standard Atmosphere.

Although the astronomical refraction model presented here

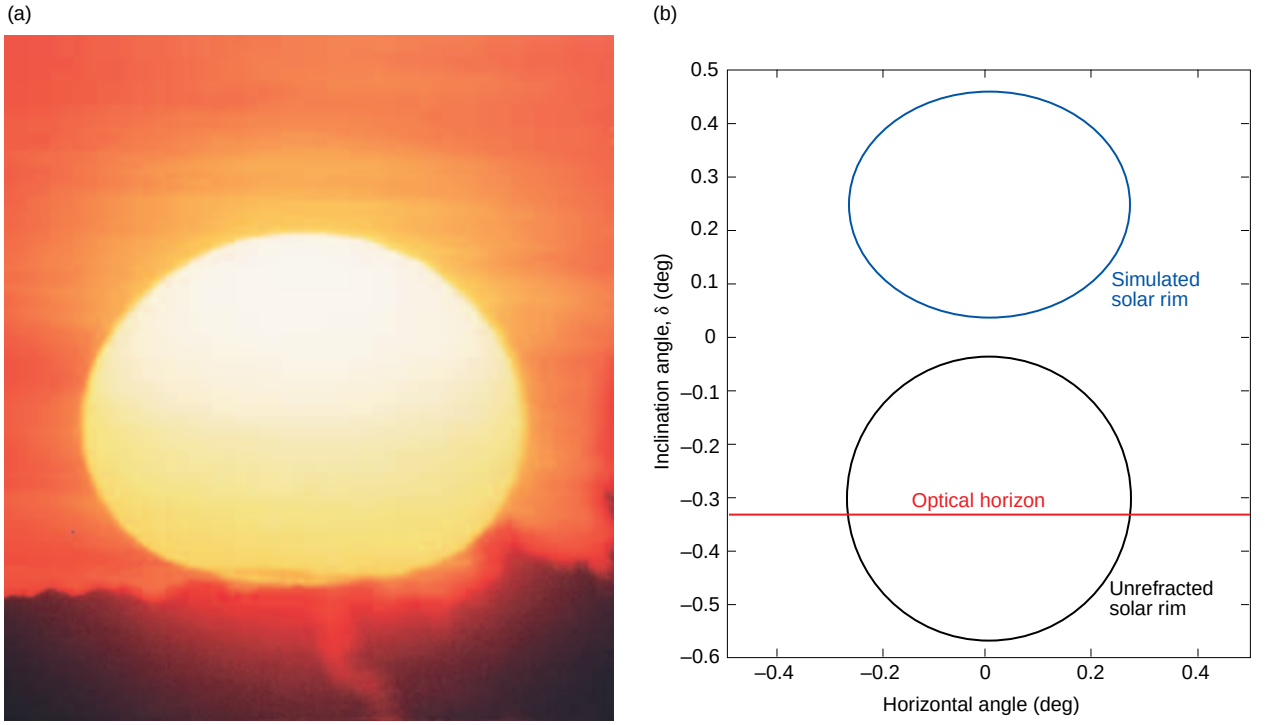

Figure 2. Comparison of (a) actual and (b) computed shapes of the setting Sun just above the horizon. The photograph was taken at an altitude of 130 m, the temperature was 31°C, and the lapse rate was −8 K/km; these values were used in the computation. (Photograph by M. E. Thomas.)

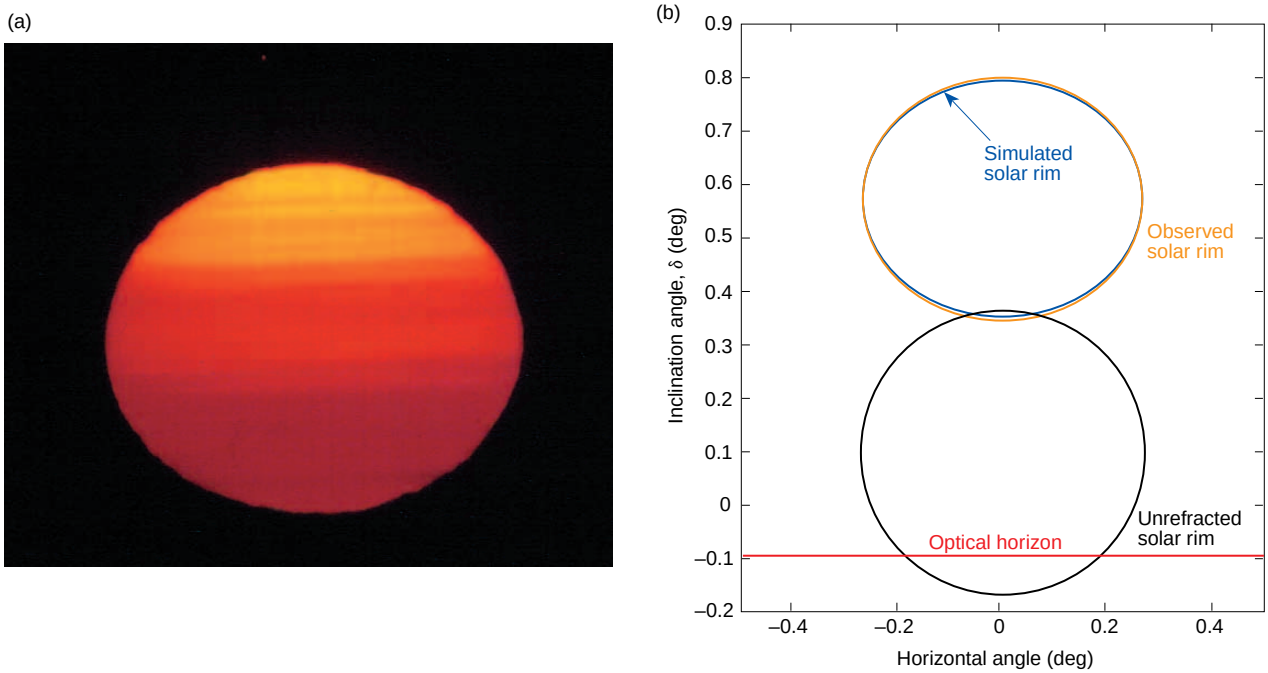

Figure 3. Comparison of an (a) observed and (b) simulated solar rim located 0.7° above the optical horizon. The model is based on a standard atmosphere and an observer at an altitude of 10 m. (Photograph courtesy of Robert Greenler/Robert Greenler Sky Photos.[8])

emphasizes visible refraction phenomena, a modified version can also be applied to the radio frequency spectral region for corrections on Global Positioning System signals. Detailed atmospheric characterization will be needed to construct the vertical refractivity profile. Such a model offers a new tool to build on the definitive work of APL scientist Helen S. Hopfield.[14]

REFERENCES

[1] Edlen, B., "The Refractive Index of Air," *Metrologia* **2,** 71–80 (1966).
[2] Lorah, L. D., and Rubin, E., "Aerodynamic Influences on Infrared System Design," in *The Infrared Handbook*, 2nd Ed., W. L. Wolfe and C. J. Zissis (eds.), Environmental Research Institute of Michigan, Ann Arbor, MI, Chap. 24 (1985).
[3] Barrell, H., and Sears, J. E., "The Refraction and Dispersion of Air for the Visible Spectrum," *Phil. Trans. Roy. Soc. London* A **238**, 1–64 (1939).
[4] Smart, W. M., *Spherical Astronomy*, 6th Ed., Cambridge University Press, Cambridge (1977).
[5] Garfinkel, B., "Astronomical Refraction in a Polytropic Atmosphere," *Astron. J.* **72**, 235–254 (1967).
[6] Hohenkerk, C. Y., and Sinclair, A. T., *The Computation of Angular Atmospheric Refraction at Large Zenith Angles*, Science and Engineering Research Council, Royal Greenwich Observatory, Hailsham, East Sussex, England, NAO Technical Note No. 63 (1985).
[7] U.S. Naval Observatory, *The Nautical Almanac*, U.S. Government Printing Office, Washington, DC (1993).
[8] Greenler, R., *Rainbows, Halos, and Glories*, Cambridge University Press, New York (1980).
[9] Schaefer, B. E., and Liller, W., "Refraction Near the Horizon," *Publ. Astron. Soc. Pac.* **102**, 796–805 (1990).
[10] Aden, A., and Meinel, M., "At Sunset," *Opt. News* **14**(11), 6 (1988).
[11] Lehn, W. H., "The Novaya Zemlya Effect: An Arctic Mirage," *J. Opt. Soc. Am.* **69**, 776–781 (1979).
[12] Kattawar, G. W., and Young, A. T., "Use of Atmospheric Refraction to Determine Temperature and Humidity Profiles in the Marine Boundary Layer," *Program of the OSA Annual Meeting*, Portland, OR, p. 81 (1995).
[13] O'Connell, D. J. K., *The Green Flash and Other Low Sun Phenomena*, North Holland Publishing Co. (1958).
[14] Hopfield, H. S., "Two-Quartic Tropospheric Refractivity Profile for Correcting Satellite Data," *J. Geophys. Res.* **74**, 4487–4499 (1969).

ACKNOWLEDGMENTS: The authors wish to acknowledge the assistance of Donald D. Duncan, Richard M. Giannola, and Helen P. Thomas during the course of this work.

THE AUTHORS

MICHAEL E. THOMAS obtained a B.E.E. from the University of Dayton in 1973, and M.S. and Ph.D. degrees from Ohio State University in 1976 and 1979, respectively. Since joining APL in 1979, he has worked on electromagnetic propagation and optical properties of materials. In 1982, he was a postdoctoral fellow in the Department of Physics at the Naval Postgraduate School. In 1988, Dr. Thomas became a faculty member of the Part-Time Programs in Engineering and Applied Science at The Johns Hopkins University G.W.C. Whiting School of Engineering, teaching courses on optical propagation and lasers. His current research interests include experimental and theoretical modeling of atmospheric propagation in the infrared, DIAL lidar, optical and infrared window materials, and the infrared properties of high-pressure gases. He has published over 65 articles in books and journals. His e-mail address is Michael.Thomas@jhuapl.edu.

RICHARD I. JOSEPH received a B.S. from the City College of the City University of New York in 1957 and a Ph.D. from Harvard University in 1962, both in physics. From 1961 to 1966, he was a senior scientist with the Research Division of the Raytheon Co. Since 1966, Dr. Joseph has been with the Department of Electrical and Computer Engineering of The Johns Hopkins University, where he is currently the Jacob Suter Jammer Professor of Electrical and Computer Engineering. During 1972, Dr. Joseph was a Visiting Professor of Physics at the Kings College, University of London, on a Guggenheim Fellowship. A member of APL's Principal Professional Staff, his research interests include electromagnetic theory, solid-state theory, statistical mechanics, the theory of nonlinear evolution equations, and oceanography. Dr. Joseph is a Fellow of the American Physical Society. His e-mail address is Richard.Joseph@jhuapl.edu.